Limnol. Oceanogr., 53(3), 2008, 1064–1075

Methylmercury cycling in estuarine sediment pore waters (Penobscot River estuary, Maine, USA)

Karen A. Merritt[1] *and Aria Amirbahman*[2]
Department of Civil and Environmental Engineering, University of Maine, Orono, Maine 04469

Abstract

Particulate mercury (Hg) sequestered in coastal marine sediments may be efficiently methylated to highly toxic methylmercury (MeHg), thereby placing exposed organisms at risk of MeHg bioaccumulation. The Penobscot River estuary in Maine, U.S.A., has been subject to Hg contamination from multiple industries including a recently closed chlor-alkali production facility. Pore-water depth profiles of total Hg, MeHg, and ancillary chemistry for the midestuary region were collected in August 2006 and June 2007. The profiles are divisible into kinetically discrete intervals with respect to MeHg dynamics. Dominant MeHg production occurs between ~2 and 7 cm in August and ~2 and 8 cm in June, with similar net MeHg production rates between 0.35×10^{-20} and 4.9×10^{-20} mol cm^{-3} s^{-1}. A significant decrease in pore-water MeHg concentration is observed in the vicinity of the sediment–water interface (SWI). For August, a minimum MeHg consumption rate constant of 1.1 d^{-1} may be estimated equal to the diffusive transport rate within a depth interval <0.75 cm. In June, the MeHg consumption zone extends from the SWI to a similar depth as for August, but the consumption rate is slower. MeHg consumption involves both sorption to sediment and demethylation. Intact sediment cores were incubated in the laboratory under various ponding regimes to study the influence of dominant geochemical parameters on in situ Hg methylation. The ponding regime changes the location of the redoxcline, which affects the depth of maximum methylation. Induced shoaling of the redoxcline brought about by the absence of any advective mixing of overlying water results in heightened MeHg efflux from the sediment.

The methylation of inorganic mercury (Hg_i) poses acute environmental concern because methylmercury (MeHg) is highly neurotoxic, and it is known to biomagnify in both terrestrial and marine food webs. Recent studies examining Hg cycling in marine ecosystems have highlighted the particular concerns posed by Hg sequestration and cycling in estuarine sediments (Hines et al. 2006; Lambertsson and Nilsson 2006). That is, through factors including the availability of pore-water sulfate (SO_4^{2-}), an abundance of labile sedimentary organic matter, and sharp redox gradients within the vicinity of the sediment–water interface (SWI), estuarine sediments may demonstrate an enhanced potential to methylate and, at least temporarily, store MeHg. Moreover, since coastal marine food webs are closely coupled to the sedimentary environment (Locarnini and Presley 1996), and sediment pore waters are frequently enriched in MeHg relative to overlying water (e.g., Choe et al. 2004), MeHg uptake by benthic and epibenthic invertebrates may present a significant and direct MeHg transport pathway to pelagic organisms.

It has been proposed that the presence of oxic or suboxic surface sediments may hinder the direct diffusive flux of MeHg across the SWI (Gagnon et al. 1996). This limitation on MeHg efflux from sediment pore water may result from either sorption to sediment solid phases in the vicinity of the SWI or an enhanced net MeHg demethylation within the same shallow depth increment. Regardless of specific mechanism, this model suggests that the potential for dissolved MeHg efflux from the sedimentary environment increases under conditions that allow the vertical migration of the oxic–anoxic boundary (i.e., the redoxcline) toward the SWI.

In this paper, we examine the diagenesis of MeHg within sediment pore waters of the Penobscot River estuary in Maine. As the processes responsible for methylation of Hg_i and consumption of MeHg frequently overlap spatially, the extant pore-water MeHg concentration defines an approximate dynamic equilibrium between production and consumption terms that is amenable to diagenetic interpretation. Using sediments from a well-characterized field site, we also incubated large-diameter cores under various ponding regimes to assess the extent to which variation in dominant geochemical parameters influences in situ Hg methylation. Specifically, this experiment tested the hypothesis that manipulation of the redoxcline depth influences the sediment depth at which maximum net methylation occurs.

The Penobscot River drains a watershed of approximately 19,350 km^2 and represents the second largest river

[1] Present address: ENVIRON International Corp., Portland, ME 04102

[2] Corresponding author (aria@umit.maine.edu; phone: (207) 581-1277; fax: (207) 581-3888).

Acknowledgments

We thank Clive Devoy and Karen Small of the Sawyer Environmental Chemistry Research Laboratory (University of Maine) for assisting in pore-water Hg analyses. Bjorn Lake, Brett Holmes, and Melinda Diehl assisted in field sampling. Two anonymous reviewers provided insightful reviews of the manuscript that greatly improved its content.

Funding for this research has been provided by the U.S. Environmental Protection Agency (STAR Fellowship 91643201), Maine Sea Grant (project NA03OAR4170054), National Oceanic and Atmospheric Administration Saltonstall-Kennedy project (NA03NMF4270124), and the Robert and Patricia Switzer Foundation. The views expressed herein are solely those of the authors and do not represent the official policies or positions of the agencies.

system in New England. The lower Penobscot River is defined by a long narrow estuary (mean width < 0.75 km), and measurable tidal influence extends 35 km upriver to the city of Bangor. As well as upriver paper mill activity, several potential point sources of Hg pollution exist within the estuary, including a recently (2000) closed chlor-alkali production facility. Sediment total Hg concentration upstream of the limit of tidal influence is <0.50 nmol Hg g^{-1} dry weight sediment (defined throughout the paper as g^{-1}), comparable with the freshwater reaches of other large New England rivers (Morgan 1998). Surface-sediment total Hg concentrations in the Penobscot estuary range between 1.25 and 27.5 nmol Hg g^{-1} (Merritt and Amirbahman 2007), and there is an extreme hot spot (2,300 nmol Hg g^{-1}) within the chlor-alkali plant discharge zone (Morgan 1998). Sediment MeHg values have not been systematically measured within the Penobscot estuary.

Materials and methods

Sediment solid phase—Sediment cores were collected in acid-leached (2 mol L^{-1} HCl) 5-cm × 30-cm polycarbonate tubes from within a 10 m^2 zone of the Frankfort Flats reach of the midestuary in close physical proximity to pore-water samplers, as described previously by Merritt and Amirbahman (2007). Total sediment Hg was determined from freeze-dried sediments by cold vapor atomic absorbance spectroscopy (CVAAS; Perkin-Elmer FIMS-400) following modified EPA method 245.5 (USEPA 1991). Spike additions and sample duplicates were run every 15 samples, and recoveries were within 4% and 7%, respectively, of the expected values. Recovery from a standard reference material (MESS-3 marine sediment) was consistently within 5% of the mean certified value (449 pmol Hg g^{-1}). The detection limit for the instrument was 0.25 nmol L^{-1}, and for the method, it was 50 pmol Hg g^{-1}, determined as three times the standard deviation of the mean of the sample blanks.

Total sediment MeHg was determined from frozen sediments by cold vapor atomic fluorescence spectroscopy (CVAFS; Tekran 2500) following modified draft EPA method 1630 (USEPA 2001*a*). Sample preparation involved acidified extraction into CH_2Cl_2, ethylation, gas chromatographic separation (HP5890), and thermal decomposition. Spike addition and sample duplicate recoveries were within 25% and 15%, respectively, of the expected values. Standard reference material (IAEA-356 sediment) recovery was within 20% of the mean certified value (27.2 pmol Hg g^{-1}). The method detection limit (MDL) was 0.3 pmol g^{-1}.

Sediments were further characterized by determination of porosity, loss-on-ignition (LOI), C : N ratio, surface area, and a range of geochemical parameters (Merritt and Amirbahman 2007). The reducible sediment Fe(III) (oxy)-hydroxide (Fe_{dith}) content was determined on each increment by dithionite extraction (Raiswell et al. 1995; Merritt and Amirbahman 2007) using inductively coupled plasma–atomic emission spectrometry (ICP-AES; Perkin Elmer Optima 3300XL). Replicate analysis was conducted on 20% of the sectioned intervals ($n = 6$), and replicate Fe recovery was ±7%.

Pore water—Pore-water samples were collected by means of multichambered (2.5-cm^3 cells on 0.75-cm centers) equilibrium dialysis frames ("peepers") as described previously (Merritt and Amirbahman 2007). Briefly, each frame contained 20 dialysis cells spaced by 0.25 cm. Frames were acid-leached (2 mol L^{-1} HCl) and then rinsed by soaking them for 2 weeks in a deionized water bath in which the water was changed every 3 d. Frames were assembled by placing a polysulfone dialysis membrane (0.22-μm Tuffryn HT-200, Gelman Sciences) across the filled cells and then securing the face plate with nylon screws. Assembled frames were immersed in a portable tank and bubbled with N_2 for 2 weeks prior to deployment. Frames designated for total Hg (Hg_T) and MeHg analyses were deployed back-to-back in marked pairs. Deployments were conducted in August 2006 and June 2007 within a mud flat (Frankfort Flats) located at the point of significant channel widening within the Penobscot estuary. For each sampling campaign, six dialysis frames were deployed within a 10-m^2 area and were continuously submerged under <10 cm of water at the lowest spring tide and ~3 m of water at the highest spring tide. Following a 30-d deployment, frames were retrieved into N_2-flushed containers and rapidly transferred into a portable N_2 glove bag set up in the field. The dialysis membrane covering each cell was rinsed, perforated with an acid-rinsed pipette tip, and the cell contents were immediately sampled for Hg_T, MeHg, dissolved sulfide (S[-II]), Fe(II), NH_4^+, base cations, pH, and dissolved organic carbon (DOC). An assessment of site variability within the 10-m^2 study area necessitated balancing the requirements of pore-water sample replication with the importance of minimizing dimensions of the dialysis frames. A discussion of variance for both pore-water and sediment solid phase analytes has been presented elsewhere (Merritt and Amirbahman 2007).

Pore-water aliquots for Hg_T were preserved with 0.5 mL of BrCl in the field and refrigerated in glass vials with Teflon-lined lids until analysis. Analysis on samples diluted to 1% BrCl was conducted by CVAFS (Tekran 2600) following EPA method 1631 (USEPA 2001*b*). The small sample volume (2.5 mL per dialysis cell) precluded the running of sample duplicates, although spike recoveries for determination for analytical bias were consistently within 4% of the expected values. Standard reference material (ORMS-3 river water) recovery was always within 6% of mean certified value (62.8 pmol L^{-1}). The MDL for diluted samples was 0.5 pmol L^{-1}.

Pore-water aliquots for MeHg were preserved with 25 μL of 25% H_2SO_4 in glass vials with Teflon-lined lids and shipped on ice to a certified laboratory (Brooks Rand, Seattle, Washington). Analysis was conducted by CVAFS (BRL Model III) following draft EPA method 1630 (USEPA 2001*a*). Sample preparation involved distillation, ethylation, chromatographic separation, and thermal decomposition. The small sample volume precluded the running of sample duplicates, although spike recoveries for determination for analytical bias were within 8% of the

Table 1. Equilibrium reactions and their corresponding constants considered in this study.

Reaction	Log K^*	Reference
$Hg^{2+} + 2HS^- \leftrightarrow Hg(HS)_2^0$	37.5†	Schwarzenbach and Widmer (1963)
$Hg^{2+} + 2HS^- \leftrightarrow HgS_2H^- + H^+$	31.5†	Schwarzenbach and Widmer (1963)
$Hg^{2+} + 2HS^- \leftrightarrow HgS_2^{-2} + 2H^+$	23.2†	Schwarzenbach and Widmer (1963)
$Hg^{2+} + HS^- \leftrightarrow HgSH^+$	30.2†	Dyrssen and Wedborg (1989)
$Hg^{2+} + HS^- \leftrightarrow HgS^0 + H^+$	26.5‡	Benoit et al. (1999)
$Hg^{2+} + DOM_s \leftrightarrow HgDOM_s$	26.7‡	Haitzer et al. (2003)
$Hg^{2+} + DOM_w \leftrightarrow HgDOM_w$	11.8§	Drexel et al. (2002)

* Ionic strength (I) and log K values as per published sources; log K corrected to $I = 0.2$ mol L^{-1} with Davies equation.
† $I = 1$ mol L^{-1}.
‡ $I = 0.1$ mol L^{-1}.
§ $I = 0.01$ mol L^{-1}.

expected values. For August 2006 sampling, standard reference material (prepared from an aliquot of DORM-2) recovery was within 3% of mean certified value (13.5 pmol L^{-1}). The MDL was 0.09 pmol L^{-1}, the mean sample-specific detection limit (SDL) was 1.2 ($\pm$0.4) pmol L^{-1}, and the sample-specific practical quantitation limit (PQL) was 3.0 ($\pm$0.9) pmol L^{-1}. For June 2007 sampling, standard reference material (prepared from an aliquot of DORM-2) recovery was within 10% of mean certified value (13.5 pmol L^{-1}). The MDL was 0.09 pmol L^{-1}, the SDL was 2.5 ($\pm$1.1) pmol L^{-1}, and the PQL was 6.2 ($\pm$2.6) pmol L^{-1}.

Sulfide (0.5 mL; detection limit 5 μmol L^{-1}; Cline 1969), Fe(II) (1 mL; detection limit 5 μmol L^{-1}; Viollier et al. 2000), and NH_4^+ (0.5 mL; detection limit 25 μmol L^{-1}; Solorzano 1969) values were determined colorimetrically by established protocols. Base cations (0.5 mL) were determined using ICP-AES; pH was measured with a portable gel probe (Accumet Gel-Filled Combination Electrode with an Orion Model 290Aplus meter) calibrated in the field at the appropriate temperature. DOC (1 mL; detection limit 20 μmol L^{-1}) was determined using a TOC analyzer (OI Corporation 700). All cation and DOC samples were acidified in the field immediately after collection. Aliquots for S(-II) determination were stabilized in 2-mL microcentrifuge tubes preloaded with 1 mol L^{-1} zinc acetate.

Intact sediment-column experiment—Large-diameter sediment columns (25 cm $\times$ 90 cm) were collected in cast acrylic tubes for a laboratory redox-manipulation experiment. Columns were driven into the sediment to a depth of ~75 cm, capped, and then dug from the mud flat with a shovel. Columns were collected from within a 5-m^2 zone of Frankfort Flats adjacent to the sampling locations described previously. Upon retrieval, the base of each column was capped, and the columns were returned to the laboratory. Columns were equilibrated in the laboratory for 3 d by continuously circulating Penobscot estuary water across the surface of the sediment. Following equilibration, two dialysis frames were deployed back to back within each column. Dialysis frames contained 20 dialysis cells (5 cm^3) spaced by 0.5 cm and were prepared for deployment as described for field-deployed frames. Columns were designated "exposed," "bubbled," and "ponded" based on the subsequent redox manipulation as follows: In the exposed column, the overlying water (~5 liters) was slowly drained after the equilibration interval, and the sediment surface was subsequently moistened daily with Penobscot estuary water. In the bubbled column, the overlying water was bubbled continuously with an aquarium pump and replaced daily to preclude SO_4^{2-} limitation. The potential for SO_4^{2-} limitation was assessed by comparison of initial measured SO_4^{2-} concentration with published maximum likely SO_4^{2-} reduction rates (King et al. 2000). Overlying water was slowly exchanged via a peristaltic pump such that the sediment surface was not subject to resuspension. In the ponded column, the overlying water was exposed to the atmosphere but not actively aerated by bubbling, and it was replaced via a peristaltic pump every 3 d. During water exchange, the sediment surface was never subaerially exposed. For both the bubbled and ponded columns, the water replacement frequency significantly exceeded the likely SO_4^{2-} reduction rate. All water used in this laboratory experiment was Penobscot estuary water collected from the vicinity of the field site at weekly intervals. The salinity of the collected water varied between 9 and 13.

Columns were maintained under the described treatments for 12 weeks at room temperature, at which point dialysis samplers were retrieved and sampled as described for Hg_T, MeHg, S(-II), Fe(II), base cations, NH_4^+, pH, and dissolved organic carbon (DOC). Small-diameter polycarbonate tubes (5 cm $\times$ 30 cm) were used to collect cores from each column. Cores were transferred into an anaerobic glove bag, sectioned at centimeter intervals, and analyzed for the reducible sediment Fe(III) (oxy)hydroxide (Fe_{dith}) content as described previously. Replicate analysis was conducted on 10% of the sectioned intervals ($n = 6$), and replicate Fe recovery was $\pm$6%.

Modeling—Equilibrium speciation modeling of Hg was conducted using PHREEQC (Parkhurst and Appelo 1999); the relevant reaction list is presented in Table 1. Equilibrium constants were corrected for Penobscot estuary conditions: $T = 15$°C using the van't Hoff equation; ionic strength = 0.2 using the Davies equation. Hg_i was calculated as $Hg_i = Hg_T - MeHg$. Complexation of Hg_i with dissolved organic matter (DOM) was modeled by considering strong (DOM_s) and weak (DOM_w) binding sites (Drexel et al. 2002; Haitzer et al. 2003). Modeling allowed for the potential precipitation of $FeS_{(s)}$, cinnabar,

and meta-cinnabar, as the generation of these solid species may limit the pore-water concentration of Hg_i. Hg-S(-II) speciation was modeled both with and without the inclusion of HgS^0. In case I, $Hg(HS)_2^0$ represents the only uncharged Hg-S(-II) species. In case II, uncharged Hg-S (-II) species are presented as the sum of $Hg(HS)_2^0 + HgS^0$. Recently, Miller et al. (2007) suggested the existence of an Hg-S(-II)-DOM complex that would result in more Hg_i binding to organic matter and a lower concentration of the uncharged Hg-S(-II) species but would not preclude its role in Hg uptake by methylating bacteria. We did not consider the Hg-S(-II)-DOM complex in this work due to the lack of thermodynamic data.

Kinetic modeling was applied to examine the competing mechanisms of production and consumption within field and laboratory column pore waters. Specifically, the computer code PROFILE (Berg et al. 1998) was used to model the vertical distribution of pore-water MeHg by a 1-dimensional mass conservation equation:

$$\left(\frac{\partial C}{\partial t}\right)_z = \frac{\partial}{\partial z}\left(\phi(D_s + D_b)\frac{\partial C}{\partial z}\right) + \alpha(\phi C_w - \phi C) + R_{net} \quad (1)$$

where C (mol cm^{-3}) is the pore-water species concentration, z is depth (positive downward from the SWI), t (s) is time; ϕ is sediment porosity, D_s ($cm^2\ s^{-1}$) is the compound-specific molecular diffusion coefficient corrected for temperature and sediment tortuosity, D_b ($cm^2\ s^{-1}$) is the sediment bioturbation coefficient, α (s^{-1}) is the sediment bioirrigation rate coefficient, C_w (mol cm^{-3}) is the concentration of the species in the overlying water, and R_{net} (mol $cm^{-3}\ s^{-1}$) is the net zero-order rate of C production or consumption. R_{net} may range from positive (net production to pore water) to negative (net consumption from pore water), and it will vary as a function of depth-specified model input values. Appropriate model input terms and model constants and constraints have been described elsewhere (Merritt and Amirbahman 2007).

PROFILE models of pore-water dynamics assume the absence of a significant advective flux and that the system is, at least, at quasi–steady state (i.e., $\frac{\partial C}{\partial t} \approx 0$). Although steady-state assumptions may not be strictly valid for environments subject to variations in salinity, bottom-water dissolved O_2, or temperature, diagenetic models such as PROFILE have allowed exploration of the depth-specific parameters that facilitate either sequestration or mobilization of sediment contaminants (Gallon et al. 2004; Goulet et al. 2007; Merritt and Amirbahman 2007).

Results and discussion

Field data—Pore water: S(-II) concentrations at the SWI were near the detection limit in August 2006 and below the detection limit in June 2007 (Fig. 1A). S(-II) values increased modestly over the top ~9 cm in August and ~15 cm in June, then increased more sharply with depth. The NH_4^+ concentration increased from 29 to 285 μmol L^{-1} in August and from 14 to 283 μmol L^{-1} in June over the depth of the pore-water profile (Fig. 1A). Dissolved Fe(II) reached maximum concentrations of ~150 and ~215 μmol L^{-1} at a depth of 1.5 cm and 0.75 cm in August and June, respectively (Fig. 1B). The DOC concentration increased from 0.3 to 1.5 mmol L^{-1} in August and from 0.4 to 0.8 mmol L^{-1} in June over the depth of the pore-water profile (Fig. 1C). Pore-water pH was consistently lower in August compared to June, with average values of 7.0 and 7.5, respectively (Fig. 1D).

Replicate pore-water MeHg profiles for August and June (Fig. 2A,B) displayed a consistently low concentration (<5 pmol L^{-1}) close to the SWI that increased to a subsurface maximum before decreasing toward the bottom of the pore-water profiles. The location and magnitude of the maximum MeHg concentration were different between profiles for both sampling intervals, although maximum concentrations varied by less than 40%. At its highest concentration, MeHg accounted for >40% of Hg_T concentration. Equilibrium modeling of Hg_i suggests that Hg-DOM complexes dominate equilibrium speciation at <10 nmol L^{-1} S(-II). Above this concentration of S(-II), Hg_i speciation is dominated by aqueous Hg-S(-II) complexes. In August and in June, for case I, $Hg(HS)_2^0$ was a relatively minor component of Hg-S(-II) species (Fig. 2A,B). In August, for case II, concentration of $Hg(HS)_2^0 + HgS^0$ species reached a maximum at ~4 cm (Fig. 2A). The highest measured pore-water MeHg concentration of 72 pmol L^{-1} occurred at a depth of ~4.5 cm, corresponding to a S(-II) concentration of 20 μmol L^{-1} (Fig. 2B). In June, for case II, concentration of $Hg(HS)_2^0 + HgS^0$ species reached a maximum at ~6.5 cm (Fig. 2B). The location of the highest measured pore-water MeHg concentration varied in each June profile (Fig. 2B) and corresponded to S(-II) concentrations ranging from 0.5 to 30 μmol L^{-1}.

Sediment solid phase: Sediment MeHg in August increased from 16.8 pmol g^{-1} at the sediment surface to 25.8 pmol g^{-1} by 4-cm depth then decreased to <0.3 pmol g^{-1} by 9-cm depth (Fig. 3). Total sediment Hg increased from 2.95 nmol g^{-1} to 4.84 nmol g^{-1} over the 0–4-cm interval then decreased to 1.22 nmol g^{-1} by 9-cm depth. MeHg values represent <0.6% of total sediment Hg throughout this depth interval. The solid-phase MeHg peak at ~4-cm depth corresponds to the zone of maximum Hg methylation. The MeHg distribution coefficient (log K_D), defined as the log ratio of solid-phase to pore-water MeHg in L kg^{-1}, was highest close to the SWI (log K_D = 3.7–3.9), and decreased nearly linearly to log K_D = 0.5–0.6 at a depth of 8.5 cm. The K_D values at depth are smaller than what is normally reported in the literature for MeHg. Recently, however, Ogrinc et al. (2007) observed log K_D values for MeHg ranging from 0.98 to 2.73 in the deep-sea surficial sediments of the Mediterranean Sea. Low K_D values may be attributed to strong complexation in the aqueous phase and to sediment quality (Ogrinc et al. 2007).

Column data: Manipulation of the redox status of the column sediments produces significant differences in the column solid-phase Fe_{dith} and pore-water S(-II) profiles (Fig. 4A,B). While all columns contain comparable Fe_{dith} at >12 cm depth (~0.8 μmol $Fe_{dith}\ g^{-1}$), the surface-

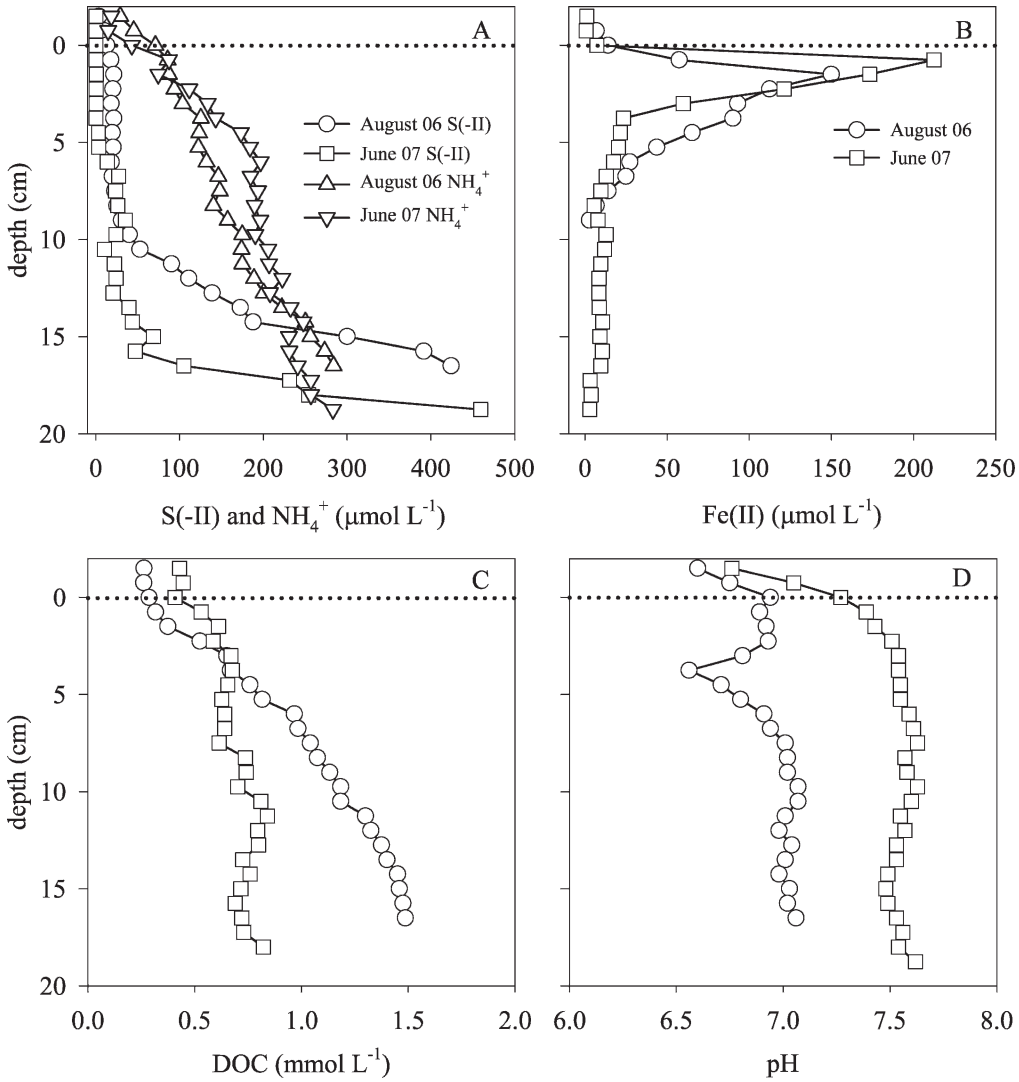

Fig. 1. Field pore-water profiles for (A) S(-II) and NH_4^+, (B) Fe(II), (C) DOC, and (D) pH.

sediment Fe_{dith} concentration varies between 13.7 μmol g^{-1} and 17.5 μmol g^{-1} for the ponded versus exposed columns, respectively, and declines by 49% (exposed), 57% (bubbled), and 75% (ponded) over the 0–4-cm depth interval (Fig. 4A). These values may be compared with the field core profile in which the surface-sediment Fe_{dith} concentration decreases by 63%, from 14.3 μmol g^{-1} to 5.4 μmol g^{-1}, over the same 0–4-cm depth interval (Fig. 4A). Similarly, in all columns, the pore-water S(-II) concentration reached ~1 mmol L^{-1} by 12.5-cm depth, although the depth of significant S(-II) increase progressively shallowed from the exposed to the bubbled to the ponded columns, respectively (Fig. 4B). Column pore-water MeHg profiles demonstrated a similar shape to field pore-water MeHg profiles—concentration increased downward from the SWI toward a subsurface maximum then decreased further down the profile (Fig. 5A–C). Similar to their respective S(-II) profiles (Fig. 4B), the MeHg concentration maxima shallowed from 9.5 cm (88 pmol L^{-1}) to 3.5 cm (67 pmol L^{-1}) to 2 cm (117 pmol L^{-1}) for the exposed, bubbled, and ponded columns, respectively. These maximum MeHg concentrations occurred at pore-water S(-II) concentrations of 760 μmol L^{-1} (exposed), 77 μmol L^{-1} (bubbled), and 625 μmol L^{-1} (ponded). In the presence of measurable S(-II), case I results demonstrated that whereas Hg_i speciation was dominated by HgS_2H^- for all columns, $Hg(HS)_2^0$ reached a maximum at a depth of 3.5 cm for the exposed and the bubbled columns and 0.5 cm for the ponded column. For case II, the depth maximums for the sum of the uncharged species $Hg(HS)_2^0$ + HgS^0 for all columns coincided with those of case I (Fig. 5A–C).

Steady-state pore-water processes—Field: Although MeHg concentrations varied between replicate pore-water profiles in August 2006, the location of the production zone boundaries was similar for both profiles. A zone of dominant net MeHg production (zone B) may be defined over 2.25–6.75-cm depth (R_{net}^{MeHg} = 0.35 to 1.1 × 10^{-20} mol cm^{-3} s^{-1}) (Fig. 2A; Table 2). Whereas measurable MeHg exists at depths <2.25 cm (zone A), the significant decrease in concentration relative to zone B

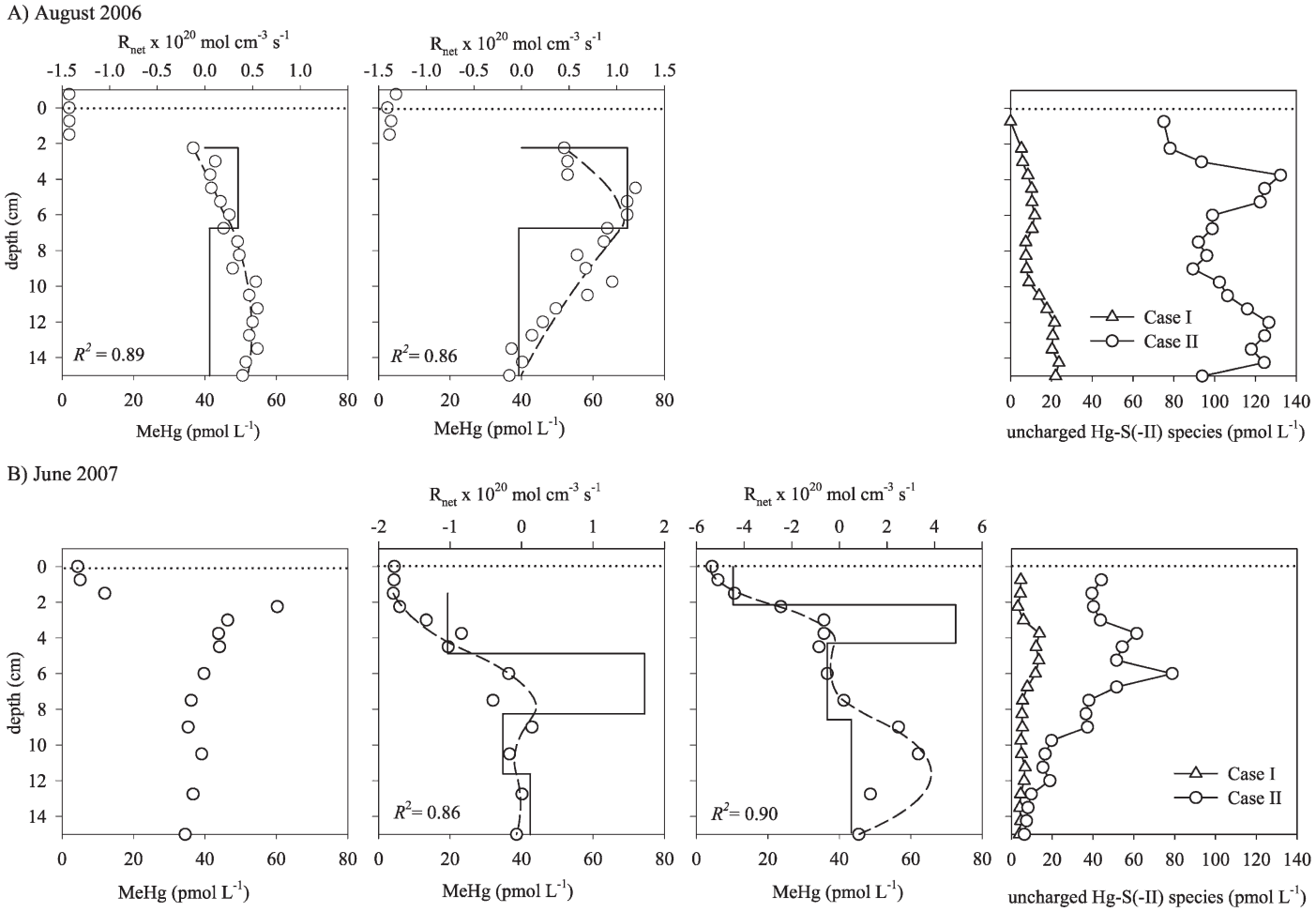

Fig. 2. (A) August 2006 and (B) June 2007 pore-water MeHg data and corresponding diagenetic pore-water profiles; circles represent field data; dashed line represents PROFILE model profile; solid line indicates model zone differentiation and net reaction rates; dotted line denotes sediment–water interface. The bottom *x*-axis corresponds to pore-water data and model profile; the top *x*-axis corresponds to model zone differentiation and net reaction rates. The figures on the right represent the pore-water $Hg(HS)_2^0$ concentrations (case I) or the sum of $Hg(HS)_2^0$ + HgS^0 concentrations (case II) as defined by thermodynamic modeling.

suggests that net MeHg consumption from pore water is occurring within the immediate vicinity of the SWI. Potential mechanisms for net MeHg consumption are discussed later. At a depth >6.75 cm (zone C), MeHg profiles show a net production rate that is significantly diminished relative to that in zone B. It is important to note that although PROFILE shows diminished MeHg production in zone C, methylation must occur to some extent at depths >7 cm in these sediments to account for the observed pore-water MeHg concentration at 15-cm depth in Fig. 2A.

For June 2007 data, there was greater heterogeneity between replicate MeHg profiles, and significant transformation processes could not always be captured by diagenetic modeling due to the extreme proximity of MeHg production and consumption zones for some profiles (Fig. 2B). For the two pore-water MeHg profiles that could be modeled, the zone of dominant net MeHg production (zone B) did not overlap between replicate profiles. Net methylation rates for these profiles ranged from $R_{\text{net}}^{\text{MeHg}} = 1.7$ to 4.9×10^{-20} mol cm^{-3} s^{-1}, where the higher net methylation rate occurred at the shallower sediment depth (<4.3 cm versus >4.9 cm) (Table 2). Whereas there was measurable MeHg at depths <2.25 cm (zone A) for all replicate profiles in June, the significant decrease in concentration relative to zone B suggests that, for June as well as for August, net MeHg consumption was occurring within the immediate vicinity of the SWI.

Zone A (0–2 cm): Possible mechanisms for the loss of MeHg from pore water within ~2 cm of the SWI include advective transport of overlying water through surface sediment, sorption to sediment solid phases, and net demethylation. If the sharp gradient in MeHg concentration observed across the zone A–B boundary is a function of physical loss terms (including diffusion and advection), one might expect the mechanism to be operative for other pore-water analytes. The fact that pore-water gradients are evident across this depth interval for in situ–generated and/or redox-sensitive analytes such as Fe(II), NH_4^+, and DOC (Fig. 1A–C) suggests that advective reoxygenation and/or

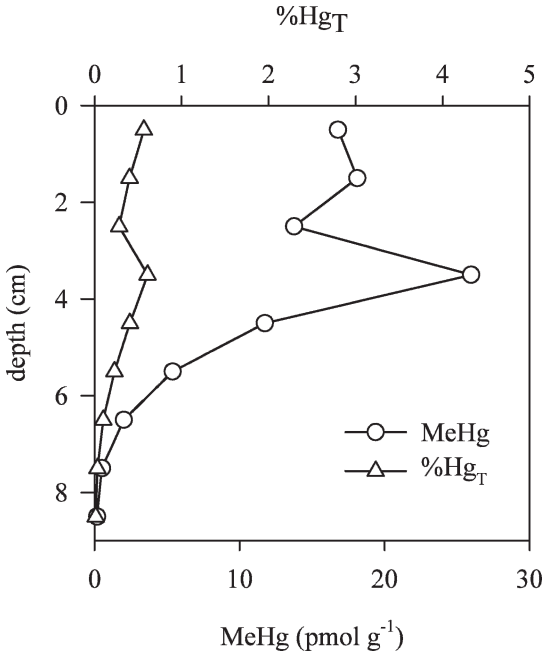

Fig. 3. Sediment solid-phase MeHg (bottom *x*-axis) and sediment solid-phase MeHg defined as a percent of total sediment solid-phase Hg (top *x*-axis) for August 2006.

pore-water dilution do not play dominant roles in generating the observed near-surface MeHg profile.

Sorption to sediment solid phases, including Fe-oxyhydroxides, sediment acid volatile sulfide (AVS), and particulate organic matter, has been proposed as a potential regulating mechanism for pore-water MeHg efflux (Bloom et al. 1999; Lambertsson and Nilsson 2006). If the net MeHg consumption in zone A is attributed entirely to adsorption, and assuming that the flux of MeHg from zone B (the zone of net MeHg production) is the sole source of MeHg to sediments in the vicinity of the SWI, Fick's First Law may be used to estimate the magnitude of that flux. Using a diffusion coefficient of 5×10^{-6} cm^2 s^{-1} (Hines et al. 2004), corrected for a porosity of 0.7 (Boudreau 1997), and an average pore-water MeHg gradient estimated from the two August profiles across the zone A–B boundary, the mean flux from zone B into zone A may be estimated at 1.7×10^{-7} pmol cm^{-2} s^{-1}. Considering the total mass of sediment MeHg in zone A (Fig. 3), it would require ~4 yr to generate the measured sediment MeHg concentration via adsorption to this zone. This calculation suggests that if the number of adsorption sites is not limiting, adsorption to surface sediments may define a pore-water MeHg sink within the vicinity of the SWI. The sediment MeHg concentration, which appears to be highest in the depth interval defined by net MeHg production (Fig. 3), supports the potential significance of adsorption as a mechanism for MeHg consumption.

What is significant for pore-water MeHg, however, is the steepness of the pore-water concentration gradient across the zone A–B boundary. A comparably steep gradient is not observed for pore-water Hg_i (Merritt and Amirbahman 2007) or any other pore-water analytes studied here

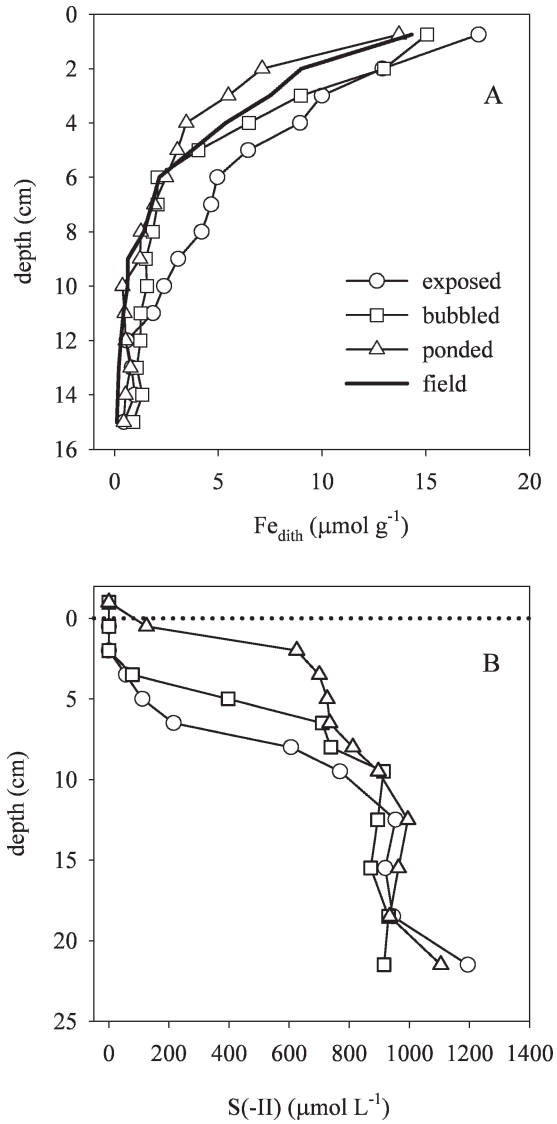

Fig. 4. (A) Field and column Fe_{dith} profiles for cores sectioned at 1-cm intervals; profiles with data points correspond to exposed, bubbled, and ponded treatments as described in the text; the profile defined by the solid line corresponds to the field profile. (B) Column pore-water profiles for S(-II); profiles correspond to exposed, bubbled, and ponded treatments as described in the text; dotted line denotes sediment–water interface.

(Fig. 1). The absence of such a gradient in pore-water Hg_i concentration may be meaningful because K_D values for Hg_i may be up to two orders of magnitude higher than K_D values for MeHg (Hammerschmidt and Fitzgerald 2004), suggesting a greater affinity of Hg_i over MeHg for sediment surfaces. If this greater affinity is the case, then although MeHg clearly appears to be associated with the sediment solid phase, adsorption is not necessarily the MeHg consumption mechanism responsible for the gradient in pore-water MeHg concentration across the zone A–B boundary. In this scenario, demethylation would be responsible for the sharp decrease in pore-water MeHg concentration within ~2 cm of the SWI, and sedimentation would explain the MeHg concentration in surface sedi-

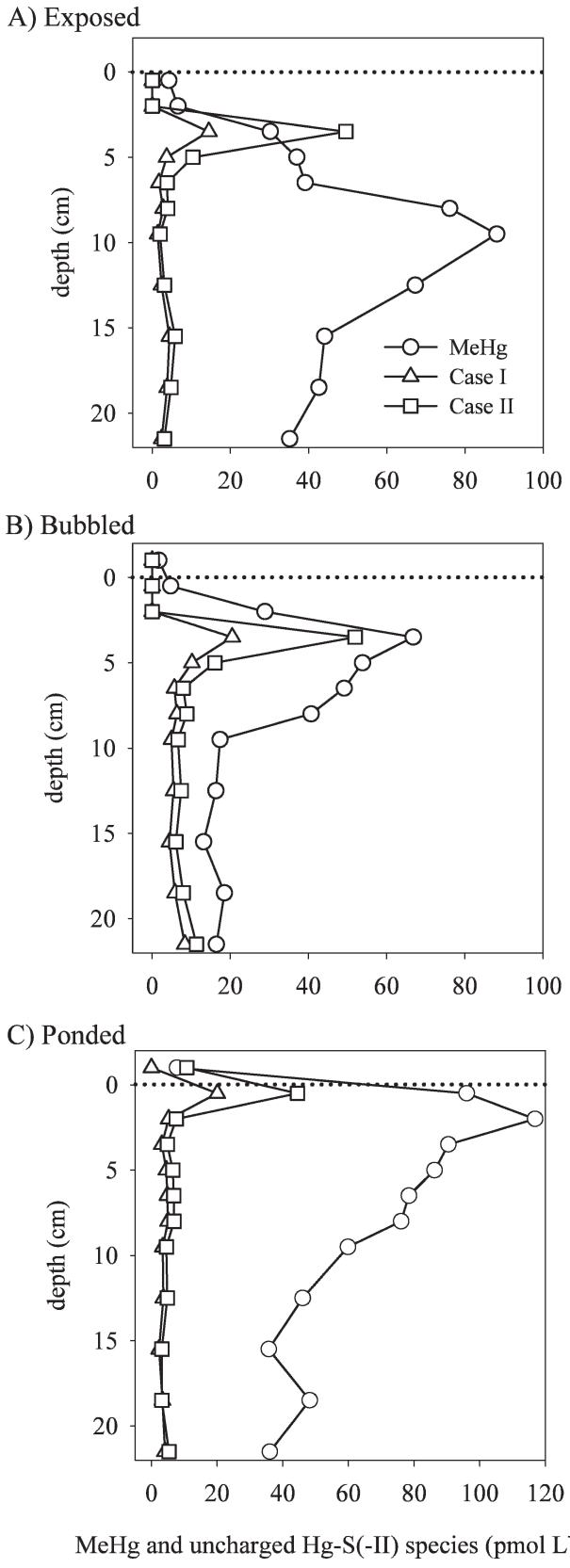

Fig. 5. Pore-water MeHg profiles for laboratory column dialysis samplers and modeled Hg-S(-II) speciation as $Hg(HS)_2^0$ (case I) or the sum of $Hg(HS)_2^0$ + HgS^0 (case II). (A) Exposed column; (B) bubbled column; (C) ponded column; treatments described in the text. Speciation is only calculated for those sediment depths with measurable S(-II) (>5 μmol L^{-1}). Note the difference in bottom *x*-axis values for the ponded column versus the exposed and bubbled columns.

Table 2. Transformation rates for field methylmercury data. All units are in mol cm^{-3} s^{-1}.

Zone	Depth interval (cm)	Reaction rate
August 2006		
A	0–2.25	4.5 to 6.5×10^{-19} (net consumption)
B	2.25–6.75	0.35 to 1.1×10^{-20} (net production)
June 2007		
A	0–4.5; 0–2.25	1.0 to 4.5×10^{-20} (net consumption)
B	4.5–8.25; 2.25–4.5	1.7 to 4.9×10^{-20} (net production)

ments. Based on an estimated site-specific sedimentation rate of 1 mm yr^{-1} (Merritt 2007), and a surface-sediment MeHg concentration of ~15 pmol g^{-1}, sedimentation of MeHg-containing particles may be responsible for all or most of the MeHg measured in surface sediments at this site. This proposed mechanism for supplying MeHg to surface sediments assumes that the demethylation rate of solid-phase MeHg is slower than the demethylation rate of pore-water MeHg.

If demethylation may explain the rapid loss of pore-water MeHg in zone A, then for August 2006 data (Fig. 2A), we can equate the minimum net MeHg consumption rate to the characteristic diffusion time estimated by $t = L^2/2\phi D_{\mathrm{MeHg}}$ (L = 0.75 cm; ϕ = 0.7; $D_{\mathrm{MeHg}} = 5 \times 10^{-6}$ cm^2 s^{-1}; Hines et al. 2004). This estimation allows us to approximate a first-order MeHg consumption rate constant of k_d = 1.1 d^{-1}. This value is within an approximate order of magnitude of published demethylation rate constants determined via isotope injection (Hintelmann et al. 2000; Marvin-DiPasquale et al. 2000; Martin-Doimeadios et al. 2004). We note that our approach to estimating an in-situ MeHg consumption rate provides a minimum value because we employ the distance on center between adjacent dialysis cells in our calculation.

With the estimated k_d value and a pore-water MeHg concentration of 37–52 pmol L^{-1} at 2.25 cm (Fig. 2A,B), a zero-order net consumption rate of -4.5 to -6.5×10^{-19} mol cm^{-3} s^{-1} may be estimated ($R^{\mathrm{MeHg}}_{\mathrm{cons[zoneA]}}$; Table 2) for the August data. This estimated net consumption rate is somewhat higher than the modeled MeHg net consumption rate for June sampling (Table 2), suggesting either a lower gross MeHg production rate or a higher gross MeHg consumption rate for August versus June sampling.

It is difficult to compare these MeHg consumption rate values directly with published rates because MeHg consumption likely includes both demethylation and sorption,

←

and few data exist regarding sorption rates of MeHg to sediment solid phases. If consumption is defined solely in terms of demethylation, demethylation rates determined from isotope-addition experiments generally calculate zero-order expressions under the assumption that all injected MeHg is equally available for demethylation. For example, zero-order demethylation rates for contaminated wetland and marsh sediments range from $\sim 10^{-16}$ to 10^{-17} mol cm^{-3} s^{-1} when calculated by multiplying the first-order demethylation rate constant (k_d; calculated based on the exponential decay of spike MeHg concentration over <12 h) by the MeHg amendment concentration or the in situ sediment MeHg concentration, respectively (Marvin-DiPasquale et al. 2003). If a zero-order demethylation rate is instead calculated by employing the in situ pore-water MeHg concentration (as opposed to the in situ sediment MeHg concentration), published rates closely approximate our zero-order estimation. Hines et al. (2006), for example, calculated a demethylation rate of 2×10^{-20} mol cm^{-3} s^{-1} for contaminated estuary sediments by following this approach. In a recent study of MeHg dynamics in a riverine wetland, Goulet et al. (2007) reported net demethylation rates ranging from 0.4 to 12.4 $\times$ 10^{-21} mol cm^{-3} s^{-1}. In most of their pore-water MeHg profiles, however, net MeHg production was observed at the SWI.

Zone B (2–8 cm): If we assume that: (1) the in situ MeHg consumption rate remains relatively constant with moderately increasing sediment depth, including with the depth-dependent progression to pore-water anoxia (*see* data in Warner et al. 2003; Hines et al. 2006; Lambertsson and Nilsson 2006), and (2) that MeHg consumption through either sorption or demethylation dominates over MeHg production within the vicinity of the SWI, we can estimate an in situ MeHg production rate for August as: $R^{\mathrm{MeHg}}_{\mathrm{prod(zoneB)}} = R^{\mathrm{MeHg}}_{\mathrm{net(zoneB)}} + R^{\mathrm{MeHg}}_{\mathrm{cons(zoneA)}} = 4.6$ to 6.6×10^{-19} mol cm^{-3} s^{-1} and for June as 2.8 to 9.3 $\times$ 10^{-20} mol cm^{-3} s^{-1}. For these estimates, $R^{\mathrm{MeHg}}_{\mathrm{net(zoneB)}} =$ 0.35 to 1.1 $\times$ 10^{-20} mol cm^{-3} s^{-1} for August and 1.7 to 4.9 $\times$ 10^{-20} mol cm^{-3} s^{-1} for June, as presented already (Table 2).

As discussed already for the MeHg consumption rate, it is difficult to directly compare the magnitude of this estimated in situ MeHg production rate with rates determined via isotope-injection experiments. Published zero-order production rate estimates frequently range between 10^{-16} and 10^{-17} mol cm^{-3} s^{-1} for experiments that measure methylation rates in pure microbial cultures (King et al. 2000) or base the zero-order production rate expression on total sediment Hg_i concentration (e.g., Marvin-DiPasquale et al. 2003; Hammerschmidt and Fitzgerald 2006). Since Hg methylation is likely limited not by availability of total sediment Hg_i, but by availability of pore-water Hg_i (Benoit et al. 1999), these published values potentially overestimate the in situ methylation rates by more than three orders of magnitude (i.e., the minimum observed pore-water K_D for Hg_i). Hines et al. (2006), for example, calculated a zero-order methylation rate of 1×10^{-19} mol cm^{-3} s^{-1} for estuary sediments based on the pore-water Hg_i concentration.

Zone C (>8 cm): For MeHg, all field profiles demonstrated decreased net methylation rates in zone C relative to zone B, although it was not possible to correlate this decline with a specific mechanism. Researchers have attributed an observed decrease in methylation rate with increasing sediment depth to either S(-II)–mediated inhibition (e.g., Gilmour et al. 1998) or the effect of diminishing substrate quality on the metabolic activity of sulfate-reducing bacteria (SRB) (King et al. 1999). Although high S(-II) concentrations may degrade the quality of labile microbial substrate (Wakeham et al. 1995) or limit microbial access to the trace metals (including Co, Ni, and Zn) required to form metabolic enzymes (Patidar and Tare, 2004), there is little consistent evidence for S(-II)–mediated toxicity to SRB at S(-II) field concentrations less than 2–3 mM (e.g., Sundback et al. 1990; Reis et al. 1992). Moreover, it is questionable whether $HgS_{(s)}$ is stably sequestered and/or microbially unavailable under sulfidic conditions (Morse and Luther 1999; Ravichandran et al. 1999; Hintelmann et al. 2000). If the concentration of uncharged Hg-S(-II) species indeed affects methylation rate linearly, some fraction of the observed significant rate decline in zone C may result from a decrease in the uncharged Hg-S(-II) species concentration at depth in the sediment (Fig. 2A,B). Any further decline in methylation rate beyond what may be explained by Hg-S(-II) speciation likely results from factors influencing the activity of the existing microbial community.

Intact-sediment-column experiment: Column redox manipulations were designed to assess the extent to which the variation in dominant geochemical parameters influences in situ Hg methylation potential. Specifically, this experiment tested the hypothesis that manipulation of the redoxcline depth influences the sediment depth at which maximum net methylation occurs. Moreover, manipulation of the redoxcline may affect MeHg efflux across the SWI. Whereas factors including warmer laboratory versus field temperatures limit direct rate comparisons between column data versus field data, comparisons may be made between individual column treatments, and results may aid field-relevant mechanistic interpretation.

In the column data, the location of the PROFILE zone boundary defining the transition from near-SWI net MeHg consumption to net MeHg production (i.e., the zone A–B inflection point defined for the field data) varies distinctly between treatments and shoals upward from 4 cm to 2.35 cm to ~0 cm for the exposed, bubbled, and ponded columns, respectively (Fig. 6A–C). The resultant compression or elimination of the net MeHg consumption zone (zone A in the field data) is consistent with the observed rise of the redoxcline toward the SWI (Fig. 4B), and it may represent an enhanced potential for pore-water MeHg efflux under progressive near-surface sediment anoxia. Whereas an approximate depth-specific correlation between elevated net methylation rate and Hg-S(-II) speciation may be supported for case I and case II in the bubbled and ponded columns (as with the field data), neither the highest pore-water MeHg concentration nor the zone of enhanced net methylation corresponds to the depth of

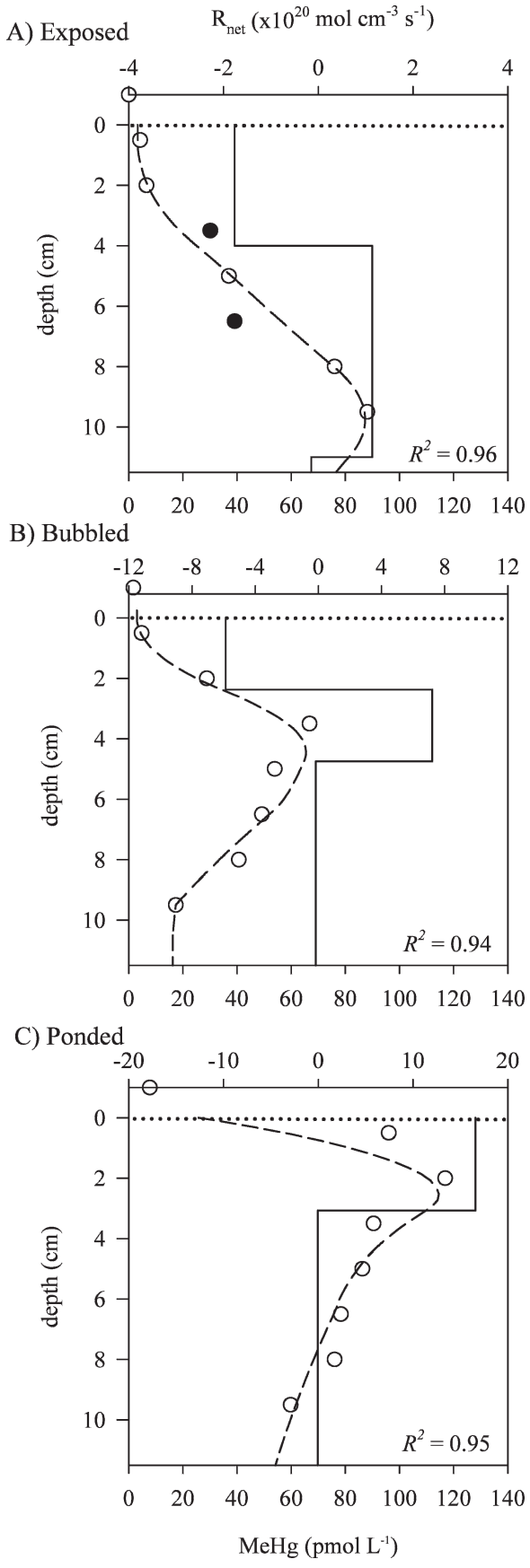

highest uncharged Hg-S(-II) species concentration in the exposed column (Fig. 5A). The offset observed may result from the enhanced oxidation of near-surface sediments under the exposed treatment. This oxidation may alter the surficial sediment chemistry and/or the microbial community structure in ways that affect Hg methylation.

As noted previously, the highest MeHg concentration measured in each column occurred at significantly varying S(-II) concentrations (77–760 μmol L^{-1} as described earlier), and the zones defined by net MeHg production ($R^{\text{MeHg}}_{\text{net}} > 0$) occurred across similarly broad ranges in pore-water S(-II) concentration. These observations of coincident net pore-water MeHg production and high S(-II) concentration are consistent with published observations (e.g., King et al. 2000; Langer et al. 2001) and suggest that simple correlations between MeHg concentration and/or methylation rate and an optimum S(-II) concentration may confound clear mechanistic interpretation of the observed methylation rate data.

The relationship between the depth of the redoxcline and the potential for shallow-sediment net MeHg production has implications for environments in which contaminant storage may be affected by hydrodynamics. In estuaries, for example, these observations suggest that across a transect defined from the subtidal zone to the adjacent salt-marsh surface, a similar contaminant concentration may be subject to both a range of potential transport mechanisms and variations in ultimate biological availability. At one extreme, in the upper intertidal zone or on the banks of salt-marsh creeks where the sediment surface may be dominantly subaerially exposed for significant periods of a lunar tidal cycle, aqueous-phase MeHg efflux may be suppressed by net demethylation or adsorption to the solid phase within the vicinity of the SWI. Biological transfer of MeHg would thus occur dominantly up the food chain through consumption of benthic infauna. At the other extreme, on the salt-marsh surface where ponded water (as in salt pans) may drive the redoxcline to or above the SWI, heightened MeHg efflux from the marsh sediment may occur. A significant pore-water MeHg flux in the absence of net near-surface demethylation or sediment adsorption may generate a distinct aqueous-phase biological exposure pathway via diffusive transfer into the overlying water.

Moreover, within the zone defined by $R^{\text{MeHg}}_{\text{net(zoneB)}} > 0$, net MeHg production increases by over an order of magnitude, from $R^{\text{MeHg}}_{\text{net(zoneB)}} = 1.1 \times 10^{-20}$ to 7.2×10^{-20} to $16.5 \times$

←

Fig. 6. Diagenetic pore-water profiles for laboratory column dialysis samplers; circles represent field data; dashed line represents PROFILE model profile; solid line indicates model zone differentiation and net reaction rates; dotted line denotes sediment–water interface. (A) Exposed column; (B) bubbled column; (C) ponded column; treatments described in the text. The bottom *x*-axis corresponds to pore-water data and model profile; the top *x*-axis corresponds to model zone differentiation and net reaction rates. Note difference in scale among all treatments for top *x*-axis data. The two filled circles in the exposed column (panel A) are excluded from model fit.

10^{-20} mol cm^{-3} s^{-1}, for the exposed, bubbled, and ponded columns, respectively (Fig. 6A–C). Since the methylation rate of Hg_i is a function of both Hg_i speciation and microbial community structure, this rate increase may not be attributed to any one simple mechanism. It appears, however, that factors that may drive progressive anoxia in surface sediments (such as in increase in labile organic matter input or surface-water temperature) may potentially increase net methylation rates. The range of such factors, which may include the frequency or extent of algal blooms, the placement of aquaculture facilities, and the warming of shallow-marine waters may have important implications for Hg cycling in the coastal zone.

References

Benoit, J. M., C. C. Gilmour, R. P. Mason, and A. Heyes. 1999. Sulfide controls on mercury speciation and bioavailability to methylating bacteria in sediment pore waters. Environ. Sci. Technol. **33:** 951–957.

Berg, P., N. Risgaard-Petersen, and S. Rysgaard. 1998. Interpretation of measured concentration profiles in sediment pore water. Limnol. Oceanogr. **43:** 1500–1510.

Bloom, N. S., G. A. Gill, S. Cappellino, C. Dobbs, L. McShea, C. Driscoll, R. Mason, and J. Rudd. 1999. Speciation and cycling of mercury in Lavaca Bay, Texas, sediments. Environ. Sci. Technol. **33:** 7–13.

Boudreau, B. 1997. Diagenetic models and their implementation. Springer-Verlag.

Choe, K.-Y., G. A. Gill, R. D. Lehman, S. Han, W. A. Heim, and K. H. Coale. 2004. Sediment–water exchange of total mercury and monomethyl mercury in the San Francisco Bay Delta. Limnol. Oceanogr. **49:** 1512–1527.

Cline, J. D. 1969. Spectrophotometric determination of hydrogen sulfide in natural waters. Limnol. Oceanogr. **14:** 454–458.

Drexel, R., M. Haitzer, J. Ryan, G. Aiken, and K. Nagy. 2002. Mercury (II) sorption to two Florida Everglades peats: Evidence for strong and weak binding and competition by dissolved organic matter released from the peat. Environ. Sci. Technol. **36:** 4058–4064.

Dyrssen, D., and M. Wedborg. 1989. The state of dissolved trace sulphide in seawater. Mar. Chem. **26:** 289–293.

Gagnon, C., E. Pelletier, A. Mucci, and W. F. Fitzgerald. 1996. Diagenetic behavior of methylmercury in organic-rich coastal sediments. Limnol. Oceanogr. **41:** 428–434.

Gallon, C., A. Tessier, C. Gobeil, and M. Alfaro-De La Torre. 2004. Modeling diagenesis of lead in sediment of a Canadian Shield Lake. Geochim. Cosmochim. Acta. **68:** 3531–3545.

Gilmour, C. C., G. S. Riedel, M. C. Ederington, J. T. Bell, J. M. Benoit, G. Gill, and M. C. Stordal. 1998. Methylmercury concentrations and production rates across a trophic gradient in the northern Everglades. Biogeochem. **40:** 327–345.

Goulet, R. R., J. Holmes, B. Page, L. Poissant, S. D. Siciliano, D. R. S. Lean, F. Wang, M. Amyot, and A. Tessier. 2007. Mercury transformations and fluxes in sediments of a riverine wetland. Geochim. Cosmochim. Acta. **71:** 3393–3406.

Haitzer, M., G. Aiken, and J. Ryan. 2003. Binding of mercury (II) to aquatic humic substances: Influence of pH and source of humic substances. Environ. Sci. Technol. **37:** 2436–2441.

Hammerschmidt, C., and W. Fitzgerald. 2004. Geochemical controls on the production and distribution of methylmercury in near-shore marine sediments. Environ. Sci. Technol. **38:** 1487–1495.

———, and ———. 2006. Methylmercury cycling in sediments on the continental shelf of southern New England. Geochim. Cosmochim. Acta. **70:** 918–930.

Hines, M. E., J. Faganeli, I. Adatto, and M. Horvat. 2006. Microbial mercury transformations in marine, estuarine and freshwater sediments downstream of the Idrija Mercury Mine, Slovenia. App. Geochem. **21:** 1924–1939.

Hines, N. A., P. L. Brezonik, and D. R. Engstrom. 2004. Sediment and porewater profiles and fluxes of mercury and methylmercury in a small seepage lake in northern Minnesota. Environ. Sci. Technol. **38:** 6610–6617.

Hintelmann, H., K. Keppel-Jones, and R. D. Evans. 2000. Constants of mercury methylation and demethylation rates in sediments and comparison of tracer and ambient mercury availability. Environ. Toxicol. Chem. **19:** 2204–2211.

King, J. K., J. E. Kostka, M. E. Frischer, and F. M. Saunders. 2000. Sulfate-reducing bacteria methylate mercury at variable rates in pure cultures and marine sediments. Appl. Environ. Microbiol. **66:** 2430–2437.

———, S. Saunders, R. F. Lee, and R. A. Jahnke. 1999. Coupling mercury methylation rates to sulfate reduction rates in marine sediments. Environ. Toxicol. Chem. **18:** 1362–1369.

Lambertsson, L., and M. Nilsson. 2006. Organic material: The primary control on mercury methylation and ambient methyl mercury concentrations in estuarine sediments. Environ. Sci. Technol. **40:** 1822–1829.

Langer, C. S., W. F. Fizgerald, P. T. Visscher, and G. M. Vandal. 2001. Biogeochemical cycling of methylmercury at Barn Island Salt Marsh, Stonington, CT, USA. Wetl. Ecol. Man. **9:** 295–310.

Locarnini, S. J. P., and B. J. Presley. 1996. Mercury concentrations in benthic organisms from a contaminated estuary. Mar. Environ. Res. **41:** 225–239.

Martin-Doimeadios, R. C. C., E. Tessier, D. Amouroux, R. Guyoneaud, R. Duran, P. Caumette, and O. F. X. Donard. 2004. Mercury methylation/demethylation and volatilization pathways in estuarine sediment slurries using species-specific enriched stable isotopes. Mar. Chem. **90:** 107–123.

Marvin-Dipasquale, M. C., J. L. Agee, R. M. Bouse, and B. E. Jaffe. 2003. Microbial cycling of mercury in contaminated pelagic and wetland sediments of San Pablo Bay, California. Environ. Geol. **43:** 260–267.

———, J. L. Agee, C. McGowan, R. Oremland, M. Thomas, D. Krabbenhoft, and C. C. Gilmour. 2000. Methyl-mercury degradation pathways: A comparison among three mercury-impacted ecosystems. Environ. Sci. Technol. **34:** 4908–4916.

Merritt, K. A. 2007. Mercury dynamics in sulfide rich sediments: Geochemical influence on contaminant mobilization and methylation within the Penobscot River estuary, Maine, USA. Ph.D. thesis, Univ. of Maine.

———, and A. Amirbahman. 2007. Mercury dynamics in sulfide-rich sediments: Geochemical influence on contaminant mobilization within the Penobscot River estuary, Maine. USA. Geochim. Cosmochim. Acta. **71:** 717–722.

Miller, C. L., R. P. Mason, C. C. Gilmour, and A. Heyes. 2007. Influence of dissolved organic matter on the complexation of mercury under sulfidic conditions. Environ. Toxicol. Chem. **26:** 624–633.

Morgan, E. 1998. Land & Water Resources Council annual report, Appendix A: Initial evaluation and recommendations on mercury in Maine. Maine Dept. of Environmental Protection.

Morse, J. W., and G. W. Luther, III. 1999. Chemical influences on trace metal-sulfide interactions in anoxic sediments. Geochim. Cosmochim. Acta. **63:** 3373–3378.

Ogrinc, N., M. Monperrus, J. Kotnik, V. Fajon, K. Vidimova, D. Amouroux, D. Kocman, E. Tessier, S. Žižek, and M. Horvat. 2007. Distribution of mercury and methylmercury in deep-sea surficial sediments of the Mediterranean Sea. Mar. Chem. **107:** 31–48.

Parkhurst, D., and C. Appelo. 1999. User's guide to PHREEQC (version 2): A computer program for speciation, batch-reaction, one-dimensional transport, and inverse geochemical calculations. U.S. Geological Survey Water Resources Investigations Report 99-4259.

Patidar, S. K., and V. Tare. 2004. Effect of micro-nutrients in anaerobic degradation of sulfate laden organics. Can. J. Civil Engin. **31:** 420–431.

Raiswell, R., D. Canfield, and R. Berner. 1995. A comparison of iron extraction methods for the determination of degree of pyritization and the recognition of iron-limited pyrite formation. Chem. Geol. **111:** 101–110.

Ravichandran, M., G. Aiken, J. Ryan, and M. Reddy. 1999. Inhibition of precipitation and aggregation of metacinnabar (mercuric sulfide) by dissolved organic matter isolated from the Florida Everglades. Environ. Sci. Technol. **33:** 1418–1423.

Reis, M. A., J. S. Almeida, P. C. Lemos, and M. J. Carrondo. 1992. Effect of hydrogen sulfide on growth of sulfate reducing bacteria. Biotech. Bioeng. **40:** 593–600.

Schwarzenbach, G., and M. Widmer. 1963. Die Loslichkeit von Metallsulfiden. I. Schwarzes Quecksilbersulfid. Helv. Chim. Acta **46:** 2613–2628.

Solorzano, L. 1969. Determination of ammonium in natural waters by the phenolhypochlorite method. Limnol. Oceanogr. **14:** 799–801.

Sundback, K., B. Jonsson, P. Nilsson, and I. Lindstrom. 1990. Impact of accumulating drifting macroalgae on a shallow-water sediment system: An experimental study. Mar. Ecol. Prog. Ser. **58:** 261–274.

U.S. Environmental Protection Agency (USEPA). 1991. Method 245.5. Revision 2.3: Determination of mercury in sediments by cold vapor atomic absorption spectrometry; methods for the determination of metals in environmental samples. U.S. Government Printing Office.

———. 2001a. Draft Method 1630. Methylmercury in water by distillation, aqueous ethylation, purge and trap, and cold vapor atomic fluorescence spectroscopy. U.S. Government Printing Office.

———. 2001b. Method 1631. Revision D: Mercury in water by oxidation, purge and trap, and cold vapor atomic fluorescence spectroscopy. U.S. Government Printing Office.

Viollier, E., P. Inglett, K. Hunter, A. Roychoudhury, and P. Van Cappellen. 2000. The ferrozine method revisited: Fe (II)/Fe (III) determination in natural waters. Appl. Geochem. **15:** 785–790.

Wakeham, S. G., J. S. S. Damste, M. E. L. Kohnen, and J. W. De Leeuw. 1995. Organic sulfur compounds formed during early diagenesis in Black Sea sediments. Geochim. Cosmochim. Acta. **59:** 521–533.

Warner, K. A., E. E. Roden, and J.-C. Bonzongo. 2003. Microbial mercury transformation in anoxic freshwater sediments under iron-reducing and other electron-accepting conditions. Environ. Sci. Technol. **37:** 2159–2165.

Received: 27 March 2007
Accepted: 10 December 2007
Amended: 18 December 2007